Supporting Information (SI)

Transport of Strontium and Cesium in Simulated Hanford Tank Waste Leachate through Quartz Sand under Saturated and Unsaturated Flow

KENTON A. ROD [1], WOOYONG UM [1, *], MARKUS FLURY [2]

1 Pacific Northwest National Laboratory

2 Washington State University, Pullman

* Corresponding author

Wooyong Um*; Pacific Northwest National Laboratory, PO Box 999, P7-22, 902 Battelle Boulevard, Richland, WA 99354

wooyong.um@pnl.gov ; phone: (509)376-4627; fax (509)376-1638

Number of Pages: 11

Number of Figures: 4

Figure SI-1. Raw data and model fit of water retention curves in quartz sand using deionized water and STWL solution.

Figure SI-2. Saturation index for cancrinite in STWL reacted with quartz sand at temperature ranging from 20 °C to 90 °C using Geochemists Workbench 7.1. Two precipitates that reach saturation or near saturation include cancrinite and Na_2SiO_4.

Figure SI-3. XRD pattern of quartz sand reacted with STWL at 90˚C. Cancrinite peaks are capped with "C".

Figure SI-4. Micro-focused XRF showing: (a) Sr (green) association with aggregates of secondary precipitates; (b) two brightest green spots used for micro-focused XRD and Fe (red) impurities on quartz. The SEM images showing: (c) reacted quartz grains containing nodules of secondary precipitates; (d) aggregates of secondary precipitates on the reacted quartz surface; (e) micro-focused XRD patterns collected from the two brightest green spots containing highest Sr concentration as shown in (b).

Hydraulic Properties of Quartz Sand Columns

Water retention curves were determined for packed quartz sand columns using the hanging water column method. The RETC computer code *(1)* was used to fit the van Genuchten water retention model to the experimental data (Equation 1S).

$$\theta_v = \theta_r + \frac{\theta_s - \theta_r}{[1+(\alpha h)^n]^{(1-n^{-1})}} \quad [1S]$$

where θ_v is the predicted volumetric water content ($cm^3\ cm^{-3}$), θ_r is the residual volumetric water content ($cm^3\ cm^{-3}$), θ_s is the saturated volumetric water content ($cm^3\ cm^{-3}$), h is the pressure head (cm), and α and n are model-estimated parameters. The estimated parameters for water were $\theta_r = 0.027$, $\theta_s = 0.38$, $\alpha = 0.039$, and $n = 7.99$ with a coefficient of correlation of $r^2 = 0.99$; for STWL were $\theta_r = 0.027$, $\theta_s = 0.38$, $\alpha = 0.036$, and $n = 10.12$ with a coefficient of correlation of $r^2 = 0.99$. The water retention curves were used to guide the adjustment of the hydraulic heads during the unsaturated flow experiments. Data for STWL were not adjusted for differences in surface tension and density of the STWL solution.

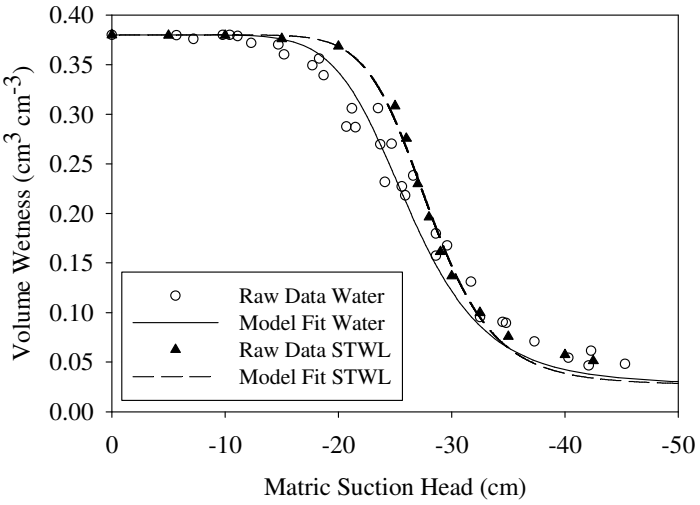

Figure SI-1. Raw data and model fit of water retention curves in quartz sand using deionized water and STWL solution.

Surface Tension Measurement

The surface tension of STWL was 75.40 ± 0.01 mN m^{-1}, measured with the Wilhelmy Plate method at 20 °C with 10 replicates, and the specific density of STWL was 1.07 g cm^{-3} at 20 ˚C. Increasing concentrations of NaOH and $NaNO_3$ increase the surface tension, and the surface tension of a mixture of 1 M NaOH and 1 M $NaNO_3$ is expected to be between 75 and 76 mN m^{-1} *(2-3)*.

Convection-dispersion equation (CDE)

The general non-equilibrium CDE is described as *(4)*:

$$\beta_s R\frac{\partial C_1}{\partial T} + (1-\beta_s)R\frac{\partial C_2}{\partial T} = \frac{1}{P}\frac{\partial^2 C_1}{\partial Z^2} - \frac{\partial C_1}{\partial Z} \quad \text{[2aS]}$$

$$(1-\beta_s)R\frac{\partial C_2}{\partial T} = \omega(C_1 - C_2) \quad \text{[2bS]}$$

$$T = \frac{vt}{L}, \qquad Z = \frac{x}{L}, \qquad C_1 = \frac{c_s}{c_o}, \qquad C_2 = \frac{c_r}{c_o} \quad \text{[2cS]}$$

$$P = \frac{vL}{D}, \qquad v = \frac{q}{\theta}, \qquad \omega = \alpha_s(1-\beta_s)\frac{RL}{v}, \qquad \beta_s = \frac{\theta + f_s\rho_b K_d}{\theta + \rho_b K_d} \quad \text{[2dS]}$$

where β_s is fraction of equilibrium sorption sites, R is the retardation coefficient, C_1 is the dimensionless concentration in the equilibrium liquid phase, C_2 is the dimensionless concentration of the rate limited sorption, T is dimensionless time, P is the Peclet number, Z is dimensionless distance, ω is the dimensionless mass transfer coefficient, v is average pore water velocity (cm day^{-1}), t is time (day), L is column length (cm), x is distance (cm), c_s is equilibrium sorption solute concentration (mol L^{-1}), c_o is the input concentration (mol L^{-1}), c_r is the rate limited sorption solute concentration (mol L^{-1}), D dispersion coefficient (cm^2 day^{-1}), q volumetric flow velocity (cm day^{-1}), α_s is the rate limited mass transfer coefficient (day^{-1}), θ is the volumetric water content (cm^3 cm^{-3}), ρ_b is the bulk density (g cm^{-3}), f is the fraction of sorption occurring in the mobile domain, and K_d is the distribution coefficient (L g^{-1}).

Geochemical Modeling

Conditions for the model used in Geochemists Workbench were 1 kg water, 2 M Na^+, 0.05 M Al^{3+}, 1.4 mM $SiO_{2(aq)}$, 0.005M CO_3^{2-}, 1 M NO_3^-, pH 14, temperature 20 to 90˚C, reacted with 20 g of quartz. Log *K* values for cancrinite were calculated using the van't Hoff equation (Equation 3aS) with the measured log *K* of -36.9 at 90˚C *(5)*. The van't Hoff equation is *(6)*:

$$ln\left(\frac{K_2}{K_1}\right) = \frac{\Delta H_r^\circ}{R}\left(\frac{1}{T_2} - \frac{1}{T_1}\right) \quad [3aS]$$

The ΔH_r for the reaction was calculated using the ΔH_f of published values *(7-9)* of the equilibrium reaction (Equation 3bS)*(5)*. For $H_2SiO_4^{2-}$, the ΔH_f was estimated using the ΔH_f of H_4SiO_4 and the ΔH_r of deprotonation from H_4SiO_4 to $H_2SiO_4^{2-}$ *(10)*:

$$Na_6Si_6Al_6O_{24}{\cdot}2NaNO_3{\cdot}4H_2O + 8H_2O + 12OH^- \leftrightarrow 8Na^+ + 6Al(OH)_4^- + 6H_2SiO_4^{2-} + 2NO_3^-;\ \log K_{90^\circ C} = -36.9 \quad [3bS]$$

The results yielded log *K* values of -44.45, -41.89, -38.96, -36.29 for temperatures 0˚C, 25˚C, 60˚C, 100˚C respectively.

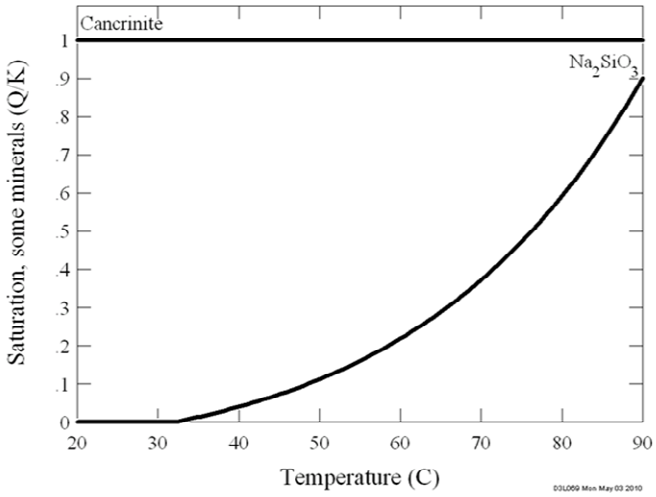

Figure SI-2. Saturation index for cancrinite in STWL reacted with quartz sand at temperature ranging from 20 °C to 90 °C using Geochemists Workbench 7.1. Two precipitates that reach saturation or near saturation include cancrinite and Na_2SiO_4.

X-ray Diffraction of Quartz Sand Reacted with STWL at 90°C

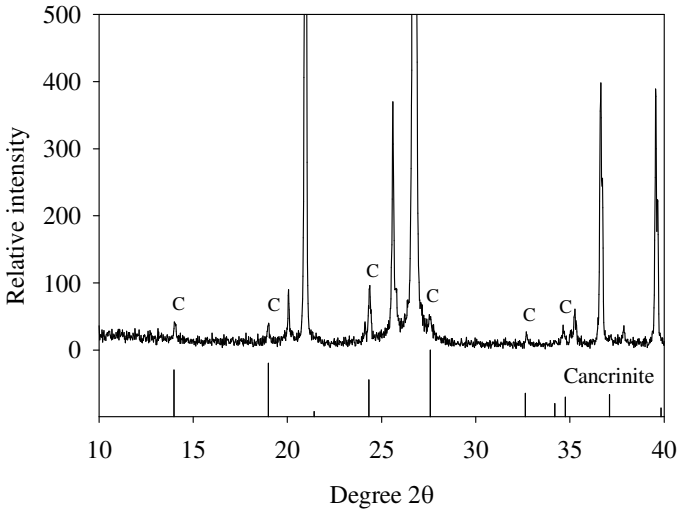

Figure SI-3. XRD pattern of quartz sand reacted with STWL at 90˚C. Cancrinite peaks are capped with "C".

Minerals were investigated with a X-ray diffractometer (XRD), Philips PW3040/00 X'pert MPD system (PANalytical, Natick, MA) with Cu Kα radiation.

Column Experiments at 75°C

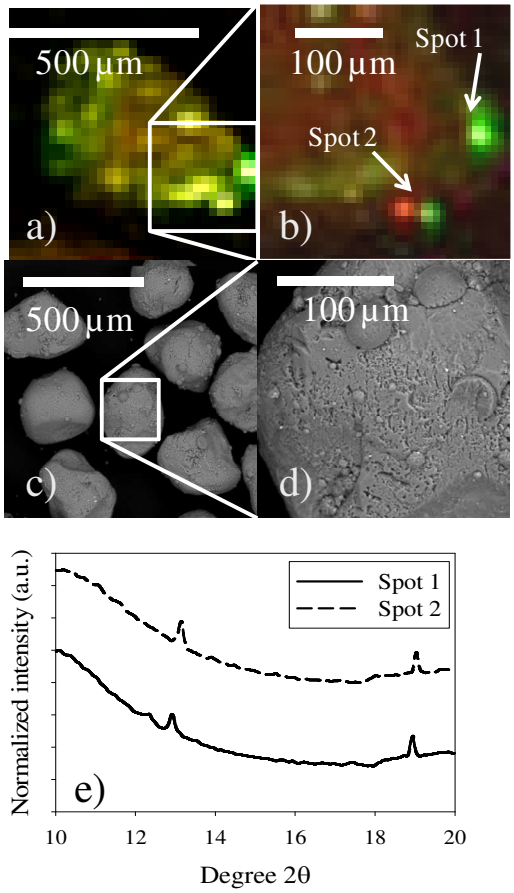

Figure SI-4. Micro-focused XRF showing: (a) Sr (green) association with aggregates of secondary precipitates; (b) two brightest green spots used for micro-focused XRD and Fe (red) impurities on quartz. The SEM images showing: (c) reacted quartz grains containing nodules of secondary precipitates; (d) aggregates of secondary precipitates on the reacted quartz surface; (e) micro-focused XRD patterns collected from the two brightest green spots containing highest Sr concentration as shown in (b).

These SEM images and XRF elemental map for Sr (green) showed that Sr was preferentially associated with secondary precipitates, as noticed as distinct nodule attached on quartz grain surface. Two micro-focused XRD patterns collected from the

brightest green colors in XRF (spot 1 and 2) showed two typical XRD peaks of 13 and 19 at 2-theta which are consistent with those found in cancrinite peaks as shown in Figure SI-3 above.

Supplemental column experiments were run with STWL under saturated flow at 75^{o}C. The temperature was controlled with heat tape wrapped around the column. Strontium concentration in the inflow was 10^{-3} M Sr and the flow rate was 4.5 pore volumes/day. Experiments were run for 30 days. Selected samples were used for synchrotron-based µ-focused XRF (Advanced Light Source, ALS, Lawrence Berkley National Laboratory) on beamline 10.3.2. Samples for XRF were prepared on Kapton tape at room temperature. Data were collected using monochromatic X-rays at 17 KeV and a spot size 10 µm. For fluorescence measurements, energy was calibrated with Fe metal by setting the first inflection on the absorption edge to 7110.75 eV. A Canberra seven-element Ge detector with XIA electron (DXP2X Model T) was used for fluorescence mapping. For micro-focused XRD, Laue patterns were collected in transmission mode using a CCD detector for two spots where the brightest green was found. The 2θ scale was calibrated with α-Al_2O_3 (corundum) with the CCD detector placed at a standardized distance from the sample (150 mm). For XRD data processing, the program FIT2D *(11)* was used to convert Laue patterns to diffractograms of 2θ versus peak intensity using a calibrated wavelength of 0.7295 Å (17 keV). Because samples are usually coarsely crystalline on the microscale and the sampled diffraction volume is small, Laue patterns from micro-XRD often have spotty and discontinuous rings. This arises from diffraction of a finite number of single crystals inside the diffracting volume and fewer individual crystals satisfying the Bragg condition compared to bulk powder

XRD. Thus, micro-diffractograms (after conversion from Laue patterns) often contain anomalous peak intensities and missing *hkl* reflections compared with the reference bulk powder diffractograms *(12)*.

Supporting Information Reference List

(1) van Genuchten, M. T.; Leij, F. J.; Yates, S. R. *The RETC code for quantifying the hydraulic functions of unsaturated soils*; IAG-DW12933934; U.S. Salinity Laboratory, U.S. Department of Agriculture: Riverside, CA, **1991**; p 85 pages.

(2) Abramzon, A. A.; Gaukhberg, R. D., SURFACE-TENSION OF SALT-SOLUTIONS. *Russ. J. Appl. Chem.* **1993,** *66*, (8), 1473-1480.

(3) Li, Z. B.; Lu, B. C. Y., Surface tension of aqueous electrolyte solutions at high concentrations - representation and prediction. *Chem. Eng. Sci.* **2001,** *56*, (8), 2879-2888.

(4) Toride, N.; Leij, F. J.; van Genuchten, M. T. *The CXTFIT code for estimating transport parameters from laboratory or field tracer experiments. Version 2.1*; Report #137; U.S. Salinity Laboratory, U.S. Department of Agriculture: Riverside, CA, **1999**; p 117.

(5) Bickmore, B. R.; Nagy, K. L.; Young, J. S.; Drexler, J. W., Nitrate-cancrinite precipitation on quartz sand in simulated Hanford tank solutions. *Environ. Sci. Technol.* **2001,** *35*, (22), 4481-4486.

(6) Langmuir, D., *Aqueous Environmental Geochemistry*. Prentice-Hall, Inc.: Upper Saddle River, New Jersey, **1997**.

(7) Liu, Q.; Xu, H.; Navrotsky, A., Nitrate cancrinite: Synthesis, characterization, and determination of the enthalpy of formation. **2005,** *87*, (2), 146-152.

(8) Benezeth, P.; Palmer, D. A.; Wesolowski, D. J., Aqueous high-temperature solubility studies. II. The solubility of boehmite at 0.03 m ionic strength as a function of temperature and pH as determined by in situ measurements. *Geochim. Cosmochim. Acta* **2001,** *65*, (13), 2097-2111.

(9) Lide, D. R., *CRC Handbook of Chemistry and Physics, 90th edition (Internet Version 2010)*. CRC Press/Taylor and Francis: Boca Raton, Florida, **2010**.

(10) Sefcik, J.; Goddard, W. A., Thermochemistry of silicic acid deprotonation: Comparison of gas-phase and solvated DFT calculations to experiment. *Geochim. Cosmochim. Acta* **2001,** *65*, (24), 4435-4443.

(11) Hammersley, A. P.; Svensson, S. O.; Hanfland, M.; Fitch, A. N.; Hausermann, D., Two-dimensional detector software: From real detector to idealised image or two-theta scan. *High Pressure Res.* **1996,** *14*, (4-6), 235-248.

(12) Manceau, A.; Marcus, M. A.; Tamura, N., Quantitative speciation of heavy metals in soils and sediments by synchrotron X-ray techniques. In *Applications of Synchrotron Radiation in Low-Temperature Geochemistry and Environmental Science.*, Fenter, P.; Rivers, M. L.; Sturchio, N. C.; Sutton, S. R., Eds. Mineralogical Society of America: Washington, D.C., **2002**; Vol. 49, pp 341-420.